Center vortex model for the infrared sector of Yang-Mills theory – Confinement and Deconfinement

M. Engelhardt* and H. Reinhardt†

Institut für Theoretische Physik, Universität Tübingen
D–72076 Tübingen, Germany

A model for the infrared sector of Yang-Mills theory based on magnetic vortices represented by (closed) random surfaces is investigated using lattice Monte Carlo methods. The random surfaces are governed by a surface area action and a curvature action. The model generates a finite-temperature deconfinement transition; the coupling constants of the model can be chosen such as to reproduce the SU(2) Yang-Mills ratio of the deconfinement temperature to the square root of the zero-temperature string tension, $T_c/\sqrt{\sigma_0} = 0.69$. This yields a physical trajectory in the space of coupling constants on which the confinement properties are approximately invariant. An at first sight surprisingly accurate prediction of the spatial string tension in the deconfined phase results, which can be made plausible in view of the specific space-time structure of the vortex configurations in this phase. The confinement properties are shown to be intimately tied to the percolation properties of the vortex surfaces.

PACS: 12.38.Aw, 12.38.Mh, 12.40.-y
Keywords: Center vortices, infrared effective theory, confinement, deconfinement transition

I. INTRODUCTION

The infrared sector of strong interaction physics is characterized by nonperturbative phenomena. Most prominent among these are the confinement of quarks and gluons into color-singlet hadrons, and the spontaneous breaking of chiral symmetry, which, through the associated (quasi-) Goldstone bosons, i.e. the pions, dominates the low-lying hadronic spectrum. On the theoretical side, there is presently convincing evidence from numerical lattice calculations [1] that Yang-Mills theory, i.e. QCD without dynamical quark degrees of freedom, indeed generates confinement. Concomitantly, diverse physical pictures of the QCD vacuum have been proposed which generate a confining potential between color sources, among others, the dual Meissner effect mechanism [2], [3], random magnetic vortices [4]- [8], the stochastic vacuum [9], the leading-log model of Adler [10], and dual QCD [11]. Other models, for instance instanton models [12], have foregone a description of confinement and concentrated on generating spontaneous chiral symmetry breaking. Furthermore, there is compelling evidence from lattice Monte Carlo experiments [1] that, as temperature is raised, one encounters a transition to a deconfined phase of Yang-Mills theory in which colored constituents can propagate over distances much larger than typical hadronic sizes.

As the above listing already indicates, there presently exists a disparate collection of model explanations for different nonperturbative QCD phenomena, but not a consistent, comprehensive picture of the degrees of freedom dominating the infrared sector. Perspectives for bridging this gap have recently arisen in the framework of the *magnetic vortex picture* of the QCD vacuum. In this picture, initially explored in [4]- [8], the Yang-Mills functional integral is assumed to be dominated by disordered vortex configurations. These vortices represent closed magnetic flux lines in three-dimensional space; correspondingly, their world sheets in four-dimensional space-time are two-dimensional. They should be contrasted with the electric flux degrees of freedom encoded by Wilson lines. In fact, they can be regarded as dual to the latter. Wilson loops are sensitive to the (quantized) magnetic flux carried by the vortices; conversely, one can think of closed vortices as measuring the electric flux carried by a Wilson line.

On a space-time lattice, this relation is particularly manifest in the fact that magnetic fluxes are defined on the lattice which is dual to the one on which Wilson lines are defined (two lattices being dual to one another means that they have the same lattice spacing a, but are displaced from one another by the vector $(a/2, a/2, a/2, a/2)$). In continuum language, using magnetic degrees of freedom means switching from the usual canonical variables, namely vector potential and electric field, to magnetic field variables along with appropriate canonical conjugates. In the magnetic language, the constraint analogous to Gauß' law is the Bianchi identity, which enforces continuity of magnetic flux.

*Supported by DFG under contract En 415/1–1.
†Supported in part by DFG under contract Re 856/4–1.

In order to emphasize the dual relation between vortices and electric flux, the above terminology, originating from the canonical framework, will be used in the following even when discussing the corresponding objects covariantly in 3+1 dimensions, i.e. including their (Euclidean) time evolution. The duality between magnetic and electric fluxes in particular provides a heuristic motivation for using vortices to describe the infrared regime of Yang-Mills theory. Whereas electric degrees of freedom become strongly coupled in the infrared, leading to the nonperturbative effects highlighted above, it conversely seems plausible to expect magnetic degrees of freedom to be weakly coupled[‡]. They can thus be hoped to furnish an adequate representation for the true infrared excitations of the theory.

Early evidence that magnetic vortices may indeed form in the Yang-Mills vacuum came from the observation that a constant chromomagnetic field is unstable with respect to the formation of tubular domains. This led to the formulation of the Copenhagen "spaghetti" vacuum [8]. Due to its technical complexity, this approach largely concentrated on local properties of vortices, as opposed to their global topological character, which will take on a decisive role in the present work. Also in the lattice formulation of Yang-Mills theory, different possibilities of defining vortices were explored [7], [14]. On this track, a number of encouraging developments have recently taken place; in particular, a practicable procedure for isolating and localizing vortices in lattice gauge configurations has been constructed [15]- [18] using an appropriate gauge[§]. This has made it possible to gather a wealth of information about these collective degrees of freedom, using lattice experiments, which was previously inaccessible. Vortices appear to dominate long-range gluonic physics not only at zero temperature [16], but also at finite temperatures [24], [25] and are able to generate both the confined as well as the deconfined phases. Moreover, there are indications that also chiral symmetry breaking is induced by vortices [26], [20], [21] and that vortices are potentially suited to account for the topological susceptibility of the Yang-Mills ensemble [22], [27], [26], [28].

If, however, the vortex picture of infrared Yang-Mills dynamics is to attain practical value beyond a qualitative interpretation of the lattice results, it must be ultimately developed into a full-fledged calculational tool, with a simplified model dynamics of the vortices allowing to concentrate on the relevant infrared physics. The work presented here is intended as an initial step in this direction. On the one hand, the effective vortex model proposed below is shown to qualitatively reproduce the confinement aspects of Yang-Mills theory, including the finite-temperature transition to a deconfined phase; on the other hand, it is verified that the parameters of the model can be chosen such as to quantitatively replicate the relation between deconfinement temperature and zero-temperature string tension known from lattice Yang-Mills experiments. Thematically, the present report is restricted to the confinement characteristics of the theory; because of this, only one genuine prediction will be presented, namely of the behavior of the spatial string tension in the deconfined phase. Another test of the predictive power of the model is discussed in a companion paper [28], which focuses on the topological susceptibility of the vortex surface ensemble proposed below. The model, which is formulated below for the case of SU(2) color, is open to many refinements in its details; however, in its present form it is entirely adequate to reproduce the vortex phenomenology hitherto extracted from lattice Yang-Mills simulations. In particular, the finite-temperature deconfinement transition can be understood in terms of a transition between two phases in which the vortices either percolate throughout (certain slices of) space-time or not.

II. VORTEX MODEL

The SU(2) vortex model under investigation in this work is defined by the following properties:

Vortices multiply any Wilson loop by a factor corresponding to a nontrivial center element of the gauge group whenever they pierce its minimal area. Center elements of a group are those elements which commute with all elements in the group; e.g. in the case of SU(2), one has the trivial phase 1 and one nontrivial element, namely the phase -1. An SU(2) color vortex thus contributes a factor -1 to a Wilson loop when it pierces the minimal area of the latter; its flux is quantized. This can be viewed as the defining property of a vortex [4]- [7] beyond any specific model assumption about its dynamics such as presented below. It specifies how vortices couple to electric fluxes, in particular the fluxes implied by the world lines of quark sources. This property provided the original motivation for the proposal of the magnetic vortex picture of confinement [4]- [6]. If the vortices are distributed in space-time sufficiently randomly, then samples of the Wilson loop of value $+1$ (originating from loop areas pierced an even number of times by vortices) will strongly cancel against samples of the Wilson loop of value -1 (originating

[‡]For Yang-Mills theory, no explicit duality transformation which manifestly exchanges strong and weak coupling regimes is known. However, in related theories, e.g. supersymmetric extensions [13], such a transformation can be constructed.

[§]For a recent discussion on the meaning of this gauge-fixing procedure and possible alternatives and generalizations, see [19]- [23]. This discussion further underscores the need to independently explore the physics of vortices, e.g. via the model presented in this work, beyond the technical discussion of how they can be identified in lattice gauge configurations.

from loop areas pierced an odd number of times by vortices), generating an area law fall-off. The circumstances under which this heuristic argument is valid will be one of the foci of the present work. As a last remark, the following should be noted. Above, the value a Wilson loop takes in a given vortex configuration was defined via the number of times the minimal area spanned by the loop is pierced by vortices. One should not misinterpret this as an arbitrariness. Due to the closed nature of the vortices, any other choice of area results in the same value for the Wilson loop. If one wishes to formulate the influence of vortices on Wilson loops in a manner which does not refer to any spanning of the loop by an area, then it is the linking number between the vortices and the loops which determines the value of the latter. For practical purposes, however, the minimal area specification is very convenient. For the purpose of finite temperature studies, note that the above specification applies equally to the area spanned by two Polyakov loops.

Vortices are closed two-dimensional random surfaces in four-dimensional (Euclidean) space-time. Vortex surfaces will be modeled as consisting of plaquettes on a four-dimensional space-time lattice. In a given lattice configuration, a plaquette can be associated with two values, 0 or 1. The value 0 indicates that the plaquette in question is not part of a vortex, whereas the value 1 indicates that it is part of a vortex. Note that this lattice is dual to the one on which "electric" degrees of freedom would be defined, such as Yang-Mills link variables, or the associated Wilson loops. How vortices emerge on the dual lattice in the framework of Yang-Mills theory via center gauge fixing and center projection is discussed in detail in [15]- [18]. The fact that vortices are closed will be implemented in the following way in numerical Monte Carlo experiments. Only Monte Carlo updates are allowed which simultaneously change the values of all the plaquettes making up the surface of an (arbitrary) three-dimensional elementary cube in the four-dimensional lattice. This can be interpreted as the creation of a vortex in the shape of the cube surface on the lattice. Such an algorithm generates only closed two-dimensional surface configurations[**]. Note that if a given plaquette which is being updated was already part of a vortex before the update, then it ceases to be part of a vortex after the update. One can think of this in terms of two vortices annihilating each other on a plaquette, if they both occupy that plaquette[††]. The net result is that the plaquette is not part of any vortex.

Vortex surfaces are associated with a physical transverse thickness. In order to represent regular, finite action, configurations in Yang-Mills theory, vortices must possess a physical transverse thickness in the directions perpendicular to the vortex surface. This thickness has furthermore been argued to be of crucial phenomenological importance, e.g. in generating the approximate Casimir scaling behavior of Wilson loops in the adjoint representation of the gauge group at intermediate distances [29], [30]. A finite vortex thickness in particular implies that it does not make sense to consider configurations in which two parallel vortex surfaces are closer to each other than the vortex thickness; i.e., vortices cannot be packed arbitrarily densely. This feature is implemented in the present vortex model simply via the lattice spacing, which forces parallel vortices to occur a certain distance from each other. This should not be misconstrued to mean that the vortices have a hard core. Rather, when two parallel vortices come too close to each other, their fluxes can be considered to annihilate in the sense that their superposition is considered equivalent to the vacuum. The reader is reminded that this is precisely the manner in which the effect of a Monte Carlo update on a vortex configuration was specified above. The algorithm thus reflects very closely the underlying physical picture. Note furthermore that the implementation of the vortex thickness via the lattice spacing implies that the latter is treated as a fixed physical scale. This will be commented upon in more detail further below. As a last remark, it should be noted that at this stage, no explicit transverse profile for the vortices has been introduced, as would be necessary e.g. for the purpose of correctly describing the behavior of adjoint representation Wilson loops [29], [30]. The vortex thickness enters only via the minimal distance between parallel vortex surfaces, whereas the surfaces themselves are still treated as infinitely thin. The introduction of an explicit transverse profile is one of the possible refinements of the model presented here.

Vortices are associated with an action density per surface area. This is reflected in a corresponding explicit term in the action, cf. eq. (4) below.

Vortices are stiff. While an ultraviolet cutoff on the space-time fluctuations of the vortex surfaces is already implied by the lattice spacing, vortices will be endowed with a certain stiffness beyond this via an explicit term in the action, cf. eq. (5) below. Specifically, if two plaquettes which share a link but do not lie in the same two-dimensional plane are both part of a vortex, then this fact will be penalized with a certain action increment. Thus, vortices are

---

[**]Note that this construction also reflects that vortex surfaces can be viewed as boundaries of three-dimensional volumes in four-dimensional space-time [22].

[††]For SU(2) color, there is only a single non-trivial center element $Z = -1$. As a consequence, two vortices annihilate, since $Z^2 = 1$. For higher SU(N) groups, where the center elements are defined by $Z^N = 1$, superposition of two vortices will in general yield a residual vortex flux, introducing the possibility of vortex branchings.

stiffer than implied by the lattice spacing alone, and the stiffness can be regulated with an independent parameter.

III. PHYSICAL INTERPRETATION OF THE MODEL

Before investigating the properties of the model vortices defined above, it is necessary to clarify more precisely which degrees of freedom these vortices are to represent. The infrared structure of typical Yang-Mills configurations is thought to be encoded in thick magnetic vortices. The term "thick" means that, whereas vortices on large scales form two-dimensional surfaces in four-dimensional space-time, they possess an extension, i.e. a regular profile function, in the directions perpendicular to the surface. This extension is one of the quantities determined in the framework of the Copenhagen vacuum [8] and also has been probed by lattice experiments [16], [18], [31]. As already mentioned in the previous section, it is instrumental in explaining the approximate Casimir scaling behavior of Wilson loops in the adjoint representation of the gauge group at intermediate distances [29], [30].

By contrast, the center projection vortices which arise in the framework of the maximal center gauges [15]- [18] are (in the continuum limit [22]) infinitely thin surfaces which provide a rough localization of the thick vortices described above, as has also been ascertained empirically using lattice experiments [16], [18]. It is possible to define the center projection vortices on arbitrarily fine lattices. Thus, while their effective action after integrating out all other Yang-Mills degrees of freedom presumably does already contain the QCD scale Λ_{QCD}, it does not yet describe an infrared effective theory; center projection vortices may still exhibit fluctuations of arbitrarily short wavelengths, within the profile of the thick vortices they represent. The QCD scale in the center projection vortex effective action merely controls on which scale this action becomes nonlocal. As one diminishes the lattice spacing, the nonlocality of the effective action presumably becomes more and more pronounced[‡‡].

Evidence for the aforementioned short wavelength fluctuations has been gathered e.g. in [31], where the binary correlations between center projection vortex intersection points with a given space-time plane were measured. This correlation function, while exhibiting the renormalization group scaling expected of a physical quantity, appears to diverge at small distances. Such behavior can be understood from short wavelength fluctuations of the center projection vortices as follows: Consider a plane which cuts a thick vortex along a (smeared-out) line, and consider furthermore intersection points of the associated center projection vortex with this plane, cf. Fig. 1. Due to the transverse fluctuations of the projection vortices, one will find a strongly enhanced probability of detecting such intersection points close to one another (compared with the probability one would expect from the mean vortex density).

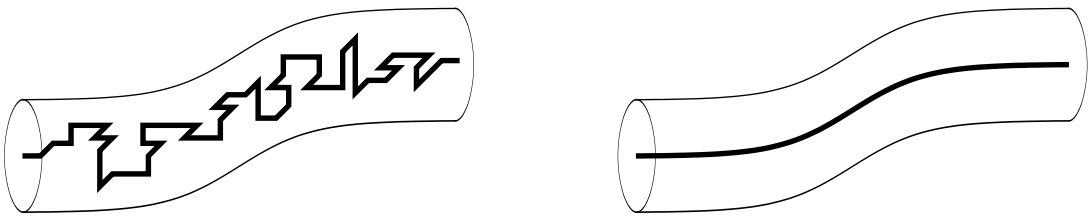

FIG. 1. Thick vortices (in a three-dimensional slice of space-time) associated with rough lattice center projection vortices (left), and smooth thin model vortices (right), respectively.

The precise location of a center projection vortex within the profile of the associated thick vortex is gauge-dependent; it changes as different specific realizations of the maximal center gauge are adopted [22], [21]. The vortex model proposed in this work does not aim to reproduce these gauge-dependent fluctuations. It is intended as a true low-energy effective theory; the model vortex surfaces defined in the previous section, while formally thin, are meant to represent the center of the profile of a thick vortex, which is smooth on short length scales, without reproducing the

[‡‡]Note that the center projection vortex effective theory, which on the lattice is a $Z(2)$ gauge theory with non-standard action, must contrive to avoid the deconfining transition well-known to occur in the standard $Z(2)$ gauge theory with plaquette action as the coupling is diminished in approaching the continuum limit.

short-wavelength fluctuations of the corresponding center projection vortex, cf. Figure 1. Alternatively, the model vortices can be interpreted as low-energy effective degrees of freedom obtained by integrating out, or smoothing[§§] over, all ultraviolet fluctuations in the abovementioned center projection vortex effective theory, down to some fixed physical scale (encoded in the vortex model via the lattice spacing). Note that such a procedure also eliminates the complicated nonlocal dynamics of the center projection vortices and leaves a vortex model action which should be well described by a few local terms, in the spirit of a gradient expansion [22]. It is this conceptual framework which led to the vortex model postulated in the previous section. Note that this picture in particular implies that one should not expect the center projection vortex density measured in lattice Yang-Mills experiments, which does obey the proper renormalization group scaling law [33] (note erratum in [24]), [18], to match the density of the model vortices. Rather, the latter should be substantially lower.

In view of this framework, it becomes clear that the lattice spacing enters the vortex model as a fixed physical cutoff scale. In other words, it is not envisaged to take the continuum limit of the model by reducing the lattice spacing and accordingly renormalizing the coupling constants. If one wishes to formulate the model in the continuum, then the lattice spacing must be replaced by some other fixed physical cutoff scale related to the thickness of the vortices. Thus, the lattice model is only insofar a caricature of continuum vortex physics as it merely allows the vortices to run parallel to the space-time axes. One could in principle remedy this e.g. by representing the vortex surfaces as triangulations in space-time, presumably again with some lower bound on the areas of the elementary triangles.

Accordingly, the lattice spacing introduces specific physical effects into the vortex model, as already mentioned in the previous section. On the one hand, the spacing accounts for aspects of the finite vortex thickness by preventing parallel vortex surfaces from occurring too close to one another. On the other hand, it introduces an ultraviolet cutoff on the space-time fluctuations of the vortices, which however is superseded by an explicit curvature penalty in the action. It must be emphasized that these effects enter the model not as unwanted lattice artefacts, but as a specific realization of physical features also present in any corresponding continuum picture of vortices.

IV. FORMAL DEFINITION

The properties of the vortex model described above can be summarized formally as follows. The basic variables are plaquettes $p_n^{\{\mu,\nu\}}$ on a four-dimensional space-time lattice, extending from a lattice site described by the four-vector n into the (positive) μ and ν directions. Note that the superscripts $\{\mu,\nu\}$, where always $\mu \neq \nu$, are unordered sets, i.e. there is no distinction between $\{\mu,\nu\}$ and $\{\nu,\mu\}$. The variables $p_n^{\{\mu,\nu\}}$ can take the values 0 or 1. Furthermore, in the following, e_μ will denote the vector in μ direction of the length of one lattice spacing. The partition function reads

$$Z = \left(\prod_n \prod_{\substack{\mu,\nu \\ \mu<\nu}} \sum_{p_n^{\{\mu,\nu\}}=0}^{1} \right) \Delta[p_n^{\{\mu,\nu\}}] \exp(-S[p_n^{\{\mu,\nu\}}]) \tag{1}$$

with the constraint

$$\Delta[p_n^{\{\mu,\nu\}}] = \prod_n \prod_\mu \delta_{L_n^\mu \bmod 2,0} \tag{2}$$

$$L_n^\mu = \sum_{\substack{\nu \\ \nu\neq\mu}} \left(p_n^{\{\mu,\nu\}} + p_{n-e_\nu}^{\{\mu,\nu\}} \right) \tag{3}$$

enforcing closedness of the vortex surfaces by constraining the number L_n^μ of occupied plaquettes attached to the link extending from the lattice site n in μ direction to be even, for any n and μ. How this constraint is conveniently enforced in Monte Carlo simulations was described in section II. The action consists of a surface area part and a curvature part, $S = S_{area} + S_{curv}$, which read

$$S_{area} = \epsilon \sum_n \sum_{\substack{\mu,\nu \\ \mu<\nu}} p_n^{\{\mu,\nu\}} \tag{4}$$

[§§] A specific smoothing procedure applied to center projection vortices in Yang-Mills theory was investigated in [32].

$$S_{curv} = \frac{c}{2} \sum_n \sum_\mu \sum_{\substack{\nu,\lambda \\ \nu\neq\mu, \lambda\neq\mu, \lambda\neq\nu}} \left(p_n^{\{\mu,\nu\}} p_n^{\{\mu,\lambda\}} + p_n^{\{\mu,\nu\}} p_{n-e_\lambda}^{\{\mu,\lambda\}} + p_{n-e_\nu}^{\{\mu,\nu\}} p_n^{\{\mu,\lambda\}} + p_{n-e_\nu}^{\{\mu,\nu\}} p_{n-e_\lambda}^{\{\mu,\lambda\}} \right) \tag{5}$$

$$= \frac{c}{2} \sum_n \sum_\mu \left[\left(\sum_{\substack{\nu \\ \nu\neq\mu}} \left(p_n^{\{\mu,\nu\}} + p_{n-e_\nu}^{\{\mu,\nu\}} \right) \right)^2 - \sum_{\substack{\nu \\ \nu\neq\mu}} \left(p_n^{\{\mu,\nu\}} + p_{n-e_\nu}^{\{\mu,\nu\}} \right)^2 \right]$$

While the lower expression for S_{curv} is more compact, the upper expression exhibits its construction more clearly: For every link extending from the lattice site n in μ direction, all pairs of attached plaquettes whose two members do not lie in the same plane are considered and, if both members are part of a vortex, this is penalized with an action increment c.

It should be noted that this type of random surface action has in recent times also attracted interest in connection with a rather different physical motivation than the one espoused in the present work [34], [35]. These investigations correspondingly focus on entirely different observables associated with the random surfaces. In particular, only what would be interpreted as the zero-temperature case in the vortex framework is considered, whereas the treatment below emphasizes also the generalization to finite temperatures and the resulting phenomena.

Wilson loops are determined by the number of times vortices pierce their minimal area. As a generic example, consider a rectangular Wilson loop with corners defined as follows. Let n_0 be an arbitrary lattice site and $m_0 = n_0 + (e_1 + e_2 + e_3 + e_4)/2$. Place the corners of the Wilson loop at $\{m_0, m_0 + Je_1, m_0 + Ke_2, m_0 + Je_1 + Ke_2\}$ with integer J, K; as already mentioned in section II, Wilson loops are defined on the lattice dual to the one the vortices are constructed on. Then, in any given vortex configuration, the number of times the minimal area spanned by this Wilson loop is pierced by vortices is

$$Q = \sum_{j=1}^{J} \sum_{k=1}^{K} p_{n_0+je_1+ke_2}^{\{3,4\}} \tag{6}$$

and the Wilson loop consequently takes the value $W = (-1)^Q$.

V. SURVEY OF THE PLANE OF COUPLING CONSTANTS

Carrying out measurements of Wilson loops of different sizes on a symmetric (16^4) lattice, one finds that the plane of coupling constants ϵ, c can be partitioned into a confining and a non-confining region, cf. Fig. 2. Since the symmetric lattice constitutes an approximation to the zero-temperature (i.e. infinite lattice) theory (the physical size of the lattice spacing will be determined further below), the confining sector is of course the one of interest.

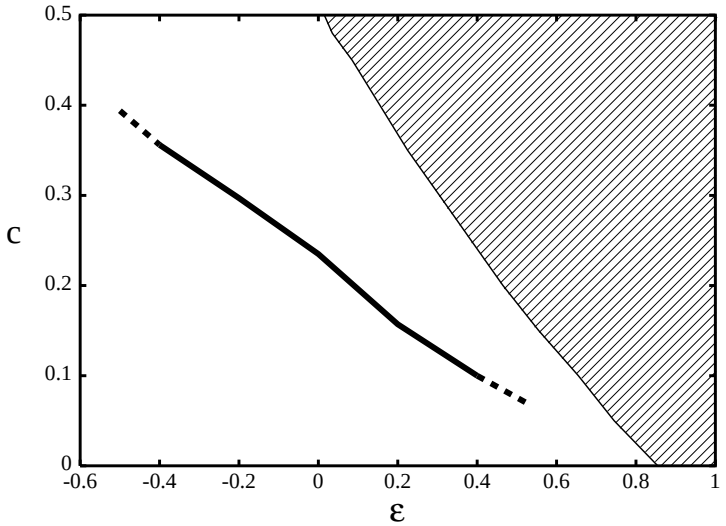

FIG. 2. Plane of coupling constants ϵ, c. The non-confining region (at zero temperature) has been shaded. The thick solid line in the confining region locates pairs of ϵ, c at which the Yang-Mills ratio $T_c/\sqrt{\sigma_0} \approx 0.69$ is reproduced by the vortex model.

Furthermore, for a large range of coupling constants ϵ, c in the confining region, one finds a deconfinement phase transition when raising the temperature of the system by decreasing the number of lattice spacings N_t making up the Euclidean time direction and evaluating the heavy quark potential using Polyakov loop correlators. Since the lattice only provides a discrete set of temperatures for given lattice spacing, it is necessary to use an interpolation procedure to determine the deconfinement temperature. For fixed ϵ, the curvature coefficient c was varied and the values of c were recorded at which the inverse deconfinement temperature crosses the values $a, 2a$ and $3a$ (a denoting the lattice spacing). Interpolation then allows to define the ratio $T_c/\sqrt{\sigma_0}$ for all c, where T_c is the deconfinement temperature and σ_0 is the zero temperature string tension. For the purpose of modeling SU(2) Yang-Mills theory, it is desirable to reproduce the value $T_c/\sqrt{\sigma_0} \approx 0.69$, cf. [36]. The line in the coupling constant plane for which this is achieved is displayed in Fig. 2. The dotted end of the line for $\epsilon > 0.4$ indicates that the $T_c/\sqrt{\sigma_0} \approx 0.69$ trajectory was not explored further into this direction, because string tension measurements became too noisy to allow its accurate determination; however, the authors have no evidence that the trajectory stops at any particular point before (presumably) ultimately reaching the non-confining region. On the other hand, in the region $\epsilon < -0.4$, the system appears to become unstable; for $\epsilon = -0.6$, unphysical oscillatory behavior of the potential between static sources can be clearly observed. This is not surprising, since for $\epsilon < 0$, the model action ceases to be manifestly positive. Only for a certain limited region of negative ϵ can one expect the model to be stabilized by the cutoff on the vortex density implied by the lattice spacing.

Setting the scale by positing a zero-temperature string tension of $\sigma_0 = (440\text{MeV})^2$, measurements of $\sigma_0 a^2$ allow to extract the lattice spacing a. The results obtained on the $T_c/\sqrt{\sigma_0} \approx 0.69$ trajectory for different values of ϵ are summarized in Table I. The lattice spacing only varies by about 10 % on the aforementioned trajectory. This corroborates the interpretation of the lattice spacing as a fixed physical quantity discussed at length in section III. It must again be emphasized that the role of the lattice spacing in the vortex model is fundamentally different e.g. from its role in lattice gauge theory. There, the lattice spacing represents an unphysical regulator, and physical quantities must be extrapolated to the continuum limit, where a certain scaling behavior connecting the coupling constant and the lattice spacing arises due to the scale invariance of the classical theory. On the other hand, in the vortex model, the $T_c/\sqrt{\sigma_0} \approx 0.69$ trajectory also implies a type of scaling behavior, but one which connects the coupling constants ϵ and c. The lattice spacing a by contrast must be counted among the physical quantities, which are to be accorded a fixed value, just like the string tension or the deconfinement temperature. Indeed, as discussed in section III, the lattice spacing has a definite interpretation connected with the transverse thickness of the vortices. It is reassuring that the lattice spacing in fact does behave accordingly on the $T_c/\sqrt{\sigma_0} \approx 0.69$ trajectory by remaining approximately constant.

Most of the measurements in the subsequent sections refer specifically to the case $\epsilon = 0$; by constraining the model to the $T_c/\sqrt{\sigma_0} \approx 0.69$ trajectory, this implies using the set of coupling constants

$$\epsilon = 0 \qquad c = 0.24 \; . \tag{7}$$

When other choices of coupling constants are used, this is explicitly stated. In particular, in the next section, a prediction of the spatial string tension in the deconfined phase will be presented; there, measurements at different points along the $T_c/\sqrt{\sigma_0} \approx 0.69$ trajectory will be taken to demonstrate the stability of the prediction.

As a final remark, note that the lattice spacing a also specifies the ultraviolet limit of validity of the effective vortex theory. In the case of the choice of coupling constants (7), one has $a = 0.39$ fm, cf. Table I, which corresponds to a maximal momentum representable on the lattice of $\Lambda = \pi/a \approx 1600$MeV.

ϵ	$\sigma_0 a^2$	a	$1/a$
0.4	0.87	0.42 fm	$1.55\,T_c$
0.2	0.84	0.41 fm	$1.58\,T_c$
0	0.755	0.39 fm	$1.67\,T_c$
-0.2	0.73	0.38 fm	$1.70\,T_c$
-0.4	0.70	0.375 fm	$1.73\,T_c$

TABLE I. Lattice spacing a for different ϵ on the $T_c/\sqrt{\sigma_0} \approx 0.69$ trajectory, cf. Fig. 2. The scale is set by positing a zero-temperature string tension of $\sigma_0 = (440\text{MeV})^2$.

VI. CONFINEMENT AND PERCOLATION

Fig. 3 displays measurements of the string tension between two static color sources, evaluated using Polyakov loop correlators, and also of the spatial string tension extracted from spatial Wilson loops, at different temperatures. These measurements quantitatively reproduce the behavior found in full Yang-Mills theory. While the correct relation between zero-temperature string tension and deconfinement temperature was fitted using the freedom in the choice of coupling constants, cf. the previous section, the behavior of the spatial string tension constitutes a first prediction of the model. As evidenced in Fig. 3, this prediction is stable to within 10 % effects as one varies the point on the physical $T_c/\sqrt{\sigma_0} \approx 0.69$ trajectory at which the measurement is taken. For the choice (7) of coupling constants, the value $\sigma_s(T = 1.67T_c) = 1.39\sigma_0$ measured in the present vortex model agrees to within 1% with the value obtained in full Yang-Mills theory, as can be inferred by interpolating the values quoted in [38]. A possible way to understand this surprisingly accurate correspondence, based on the specific space-time structure of the vortex configurations in the deconfined phase, will be discussed further below.

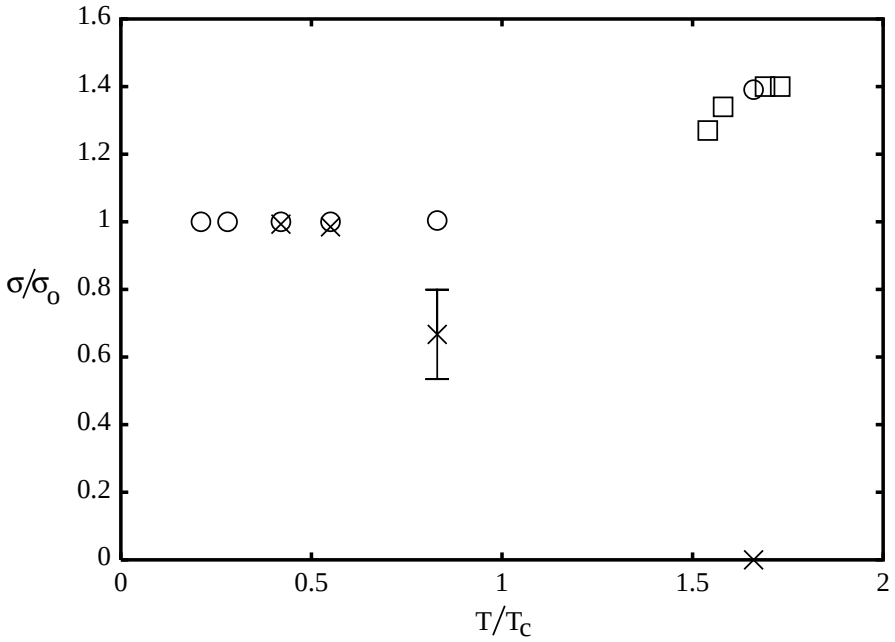

FIG. 3. String tension between two static color sources (crosses) and spatial string tension (open symbols) as a function of temperature. Circles denote measurements taken for $\epsilon = 0, c = 0.24$, whereas squares are measurements taken at other points on the $T_c/\sqrt{\sigma_0} \approx 0.69$ trajectory, namely for $N_t = 1$ at $\epsilon = 0.4, 0.2, -0.2, -0.4$ (in order of ascending T/T_c), cf. Table I. All but one of the measurements displayed have errors smaller than the symbols by which they are represented and result from fitting linear functions to the extracted potentials at each temperature; this described well all data taken at the temperature in question. The exception is the measurement of the string tension between two color sources at $0.83T_c$. There, a simple linear fit fails, and logarithmic and/or Coulomb terms were added to fit the data taken. It should be noted that logarithmic terms are indeed known to play a role in the static quark potential at finite temperatures and they become appreciable near $T = T_c$, cf. [37] . While such a more general ansatz allows an acceptable fit, the string tension extracted depends on the precise ansatz to the extent indicated by the error bar in the figure.

In order to understand and interpret the confinement properties displayed in Fig. 3, it is useful to contrast them with the percolation properties of the vortices [25]. To best exhibit the latter, it is necessary to consider three-dimensional slices of the lattice universe (where the slices are taken *between* two parallel hyperplanes of the lattice on which the vortices are defined). On such slices, vortices form closed lines made up of links. Both time slices as well as slices in which one of the spatial coordinates is fixed (in the following referred to as space slices) are of interest. By finding an initial vortex link, identifying all vortex links connected to it, and iterating this procedure with all new vortex links reached, one can discriminate between disjoint vortex clusters; the space-time extension of a cluster is then defined as the maximal Euclidean distance between two points on that cluster. In a percolating ensemble, most vortex links will be organized into clusters of near maximal size, which corresponds to an extension of $\sqrt{N_t^2 + 2N_s^2}/2$ lattice spacings on a $N_t \times N_s \times N_s$ space slice due to the periodic boundary conditions (and analogously for time slices). On the other hand, in the absence of percolation, most vortex links will be organized into small clusters.

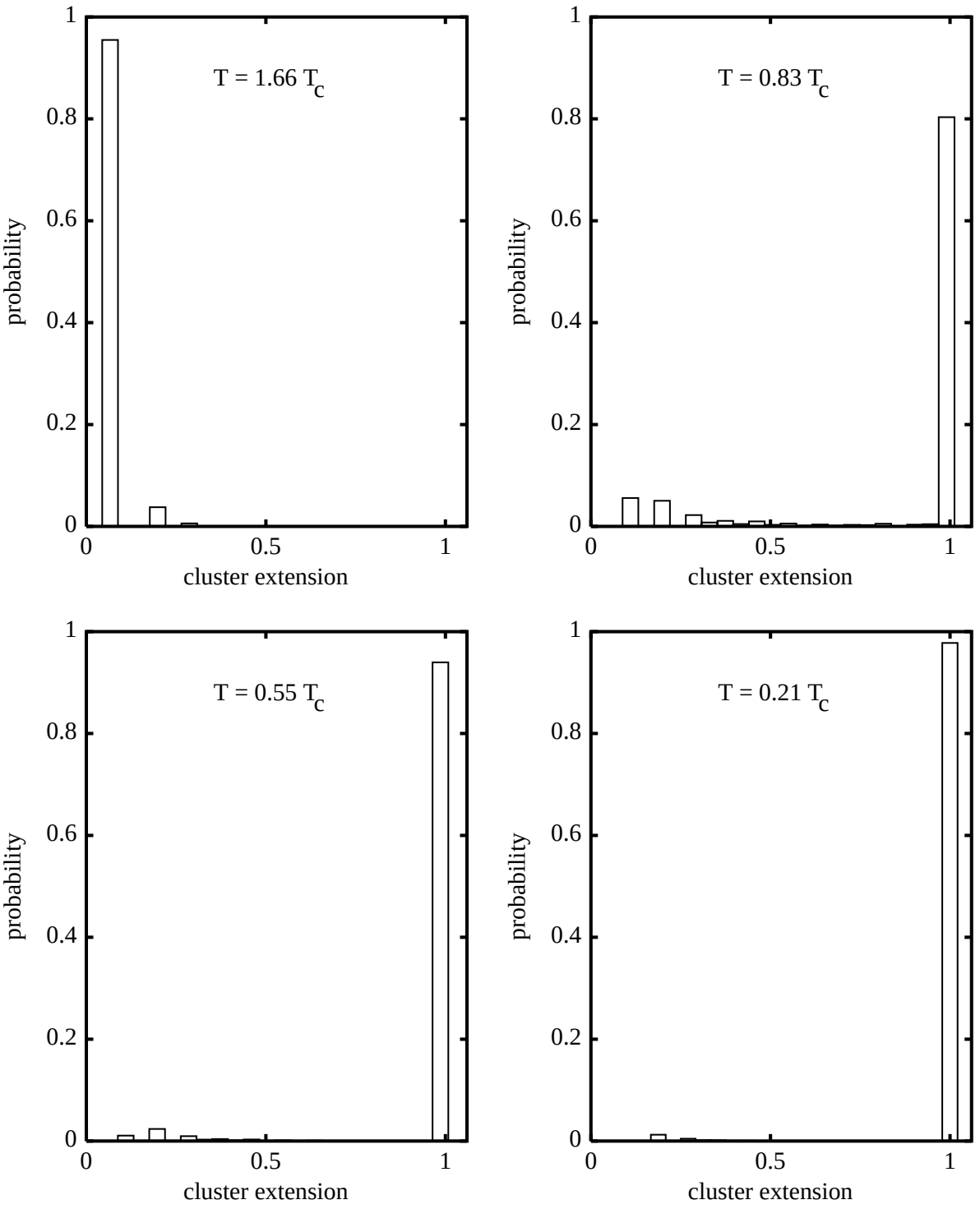

FIG. 4. Vortex links found in space slices of the random vortex surfaces, binned according to the extension of the cluster to which they belong (given in units of the maximal possible extension $\sqrt{N_t^2 + 2N_s^2}a/2$). The distributions were normalized to unity, so that each bar represents the fraction of vortex links found in clusters of the corresponding extension.

Fig. 4 displays, for different temperatures and taking space slices of the lattice universe, the fraction of vortex links present in the ensemble which are part of a cluster of the extension specified on the horizontal axis. Clearly, in the confining phase, vortices in space slices percolate, whereas they cease to percolate in the deconfined phase. A different picture is obtained when considering time slices, cf. Fig. 5. There, vortex lines percolate in both phases.

This in particular also implies that the two-dimensional vortex surfaces in four-dimensional space-time percolate in both phases. Only when considering space slices of the lattice universe does a percolation transition become visible.

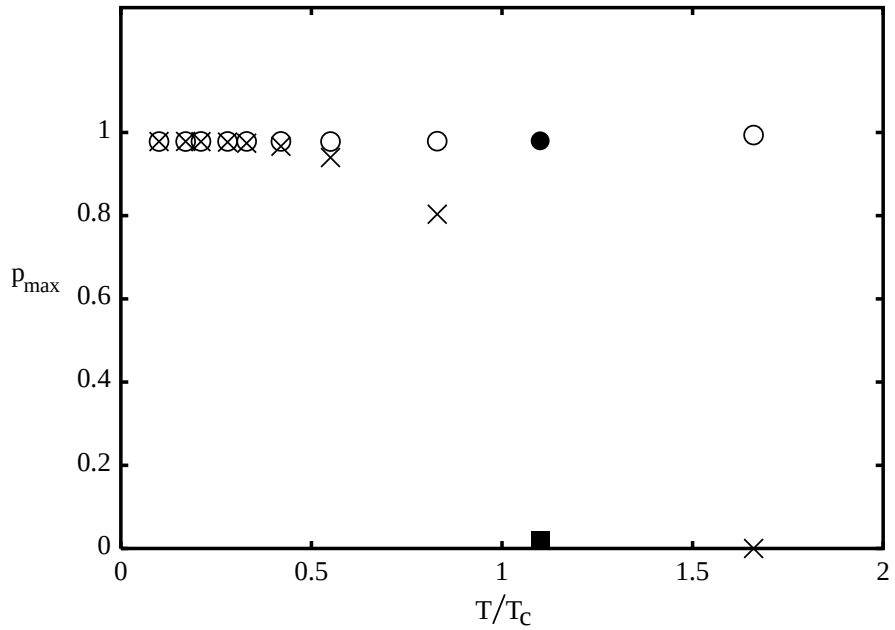

FIG. 5. Fraction p_{max} of vortex links which belong specifically to clusters whose extension lies within (roughly) 5% of the maximal possible extension (cf. the width of the bins in Fig. 4), as a function of temperature. Open circles show p_{max} measured in time slices of the random vortex surfaces present in the ensemble, crosses show for comparison the values found in space slices (i.e. the crosses correspond to the heights of the bins of maximal cluster extension in Fig. 4). The measurements at $T = 1.1T_c$ (full circle representing time slice and square representing space slice) were obtained by an interpolation procedure, see text. Evidently, clusters in time slices of the lattice universe percolate even in the deconfined phase. Note how the behavior of p_{max} parallels the behavior of the corresponding string tensions, cf. Fig. 3.

Measurements at fixed ϵ, c (and therefore at fixed lattice spacing a) only provide a discrete set of temperatures; in the case of $\epsilon = 0, c = 0.24$ treated above, $N_t = 2$ happens to correspond to $T = 0.83T_c$, whereas $N_t = 1$ corresponds to $T = 1.67T_c$ (the reader may feel uneasy at this point because $N_t = 1$ seems rather special, and the observed phenomena in the deconfined phase may be tied to this particular case; this concern is addressed in more detail further below). Clearly, it is desirable to have a better temperature resolution especially in the region of the phase transition. Values of observables at intermediate temperatures can be defined via an interpolation procedure such as already employed in section V. This is how the values at $T = 1.1T_c$ in Fig. 5 were obtained. The measurements in section V in particular allowed to interpolate, for fixed $\epsilon = 0$, the value of $T_c a$ as a function of c. This, however, also permits finding the set of c_i for which $1.1 = (Ta)/(T_c a) = 1/(iT_c a)$, with i denoting an integer. Then, by construction, measurements of an observable on a lattice with $N_t = i$ at coupling $c = c_i$ all correspond to $T = 1.1T_c$, which again by interpolation allows to define the observable also for $c = 0.24$ at $T = 1.1T_c$.

A more specific picture of the deconfined phase is obtained by analyzing the number of links contained in the clusters. For the choice of coupling constants $\epsilon = 0, c = 0.24$, (only) the lattice universe with $N_t = 1$ realizes the deconfined phase. On space slices of this lattice, clusters containing only one vortex link are necessarily clusters which wind around the lattice in the Euclidean time direction and are closed by virtue of the periodic boundary conditions. The smallest non-winding vortex cluster by contrast contains four links. Indeed, measuring the percentage of links belonging to clusters containing only one link yields a fraction of 95% (for $N_t = 1$, i.e. $T = 1.67T_c$). Thus, the small extension vortex clusters which dominate the deconfined phase can more specifically be characterized as winding vortex configurations.

Note that this specific space-time structure of the vortex configurations in the deconfined phase, which is also found for the center projection vortices extracted from the SU(2) Yang-Mills ensemble, cf. [25], may explain the surprising accuracy of the prediction of the spatial string tension displayed in Fig. 3. Given that the Yang-Mills dynamics favors the formation of winding vortices extending predominantly into the Euclidean time direction, the vortex surfaces allowed in the present model can quite accurately represent the configurations relevant in the full theory, despite the large lattice spacing. Thus, in this particular setting, the model space does not imply a strong truncation of the full

physics, even on the coarse lattice used.

The reader may feel uneasy about the discussion in the previous paragraphs because the lattice with $N_t = 1$ realizing the deconfined phase seems a rather special case, and one might worry that the loss of percolation, and more specifically the dominance of winding vortices, is a particular feature of the $N_t = 1$ lattice. In order to show that, on the contrary, the correlation between deconfinement on the one hand and the dominance of winding vortices on the other hand is a generic feature of the random vortex surfaces, the authors have numerically investigated the (unrealistic) choice of parameters $\epsilon = 0, c = 0.46$. In this case, lattices with $N_t = 1, 2, 3$ realize the deconfined phase, whereas lattices with larger N_t realize the confined phase (as determined by measurements of the string tension). Table II displays the resulting fraction p_i of vortex links found in clusters containing a total of i links.

For $N_t = 1$, the winding vortices containing one link dominate the ensemble to more than 99.5%. For $N_t = 2$, at least 77% of links detected were part of a winding vortex containing a total of two links; the fraction p_4 contains additional winding vortices (with a transverse fluctuation), but the analysis is ambiguous, since there are also non-winding clusters containing four links. For $N_t = 3$, this ambiguity does not occur, and the fractions p_3, p_5 and p_7 necessarily correspond to winding vortices, with transversal fluctuations in the cases of p_5 and p_7. Thus, winding vortices still encompass well more than half of the vortex links present in the ensemble even quite near the critical temperature (additional winding vortices are subsumed in the further odd fractions $p_9, p_{11}, \ldots$ not shown). Percolating clusters (embodied in p_{max}) on the other hand are virtually non-existent for the deconfined cases $N_t = 1, 2, 3$. By contrast, for $N_t \geq 4$, which corresponds to the confining phase, the dominant proportion of vortex links is associated with percolating vortices (cf. p_{max}). Short winding vortices completely disappear, including ones with small transverse fluctuations (cf. p_5 and p_7 in the case $N_t = 5$).

As a last point, it is interesting to contrast the percolation phenomena exhibited above with the behavior of the vortices in the region of the phase diagram in which confinement is absent even at zero temperature (the shaded region in Fig. 2). In the cases studied further above, taken from the confining regime of the coupling constant plane, a percolation transition at the deconfinement temperature T_c only became visible in space slices of the lattice universe; on the other hand, percolation of vortex lines in time slices, and consequently percolation of the complete vortex surfaces in four dimensions, persisted even above the deconfinement temperature T_c. In contradistinction to this, in the non-confining regime of the coupling constant plane, the two-dimensional vortex surfaces in four-dimensional space-time as a whole do not percolate. Note that this is equivalent to the statement that vortex lines do not percolate in *any* three-dimensional slice of space-time (at zero temperature, or any symmetric lattice approximation of it, there is of course no distinction between space and time slices). As a case in point, therefore, Fig. 6 displays the sliced vortex distribution analogous to Fig. 4, but evaluated using a symmetric (16^4) lattice for $\epsilon = 0.17, c = 0.4$, which is in the non-confining region, cf. Fig. 2.

N_t	p_1	p_2	p_3	p_4	p_5	p_6	p_7	p_{max}
1	1.00	0	0	0	0	0	0	0
2	0	0.77	0	0.14	0	0.06	0	0
3	0	0	0.41	0.07	0.08	0.06	0.05	0
4	0	0	0	0.04	0	0.02	0	0.84
5	0	0	0	0.02	0	0.01	0	0.89
6	0	0	0	0.02	0	0.01	0	0.91
7	0	0	0	0.02	0	0.01	0	0.92
8	0	0	0	0.02	0	0.01	0	0.92

TABLE II. Fraction p_i of vortex links found in clusters containing a total of i links, as measured by taking space slices of the $\epsilon = 0, c = 0.46$ random vortex surface ensemble on lattices with a temporal extension $N_t a$. For these values of the coupling constants, $N_t = 1, 2, 3$ realize the deconfined phase, whereas higher N_t correspond to the confining phase. For comparison, the table also quotes the fraction p_{max} of links found in clusters whose extension lies within (roughly) 5% of the maximal possible space-time extension (cf. the width of the bins in Fig. 4).

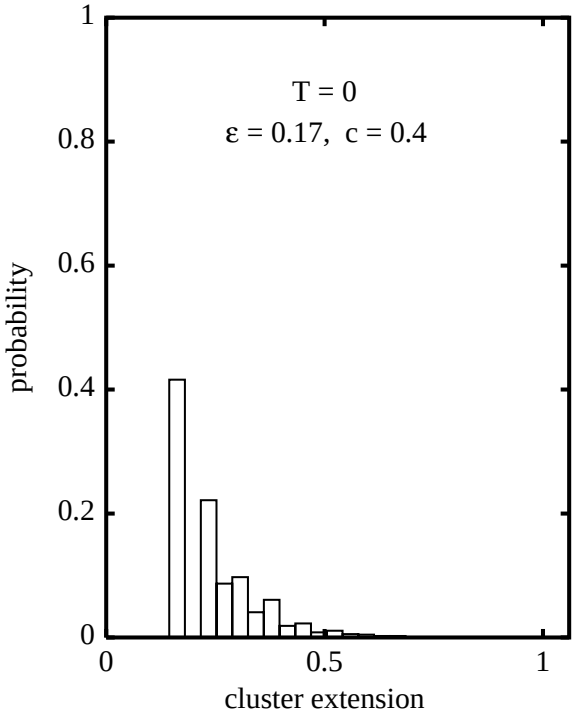

FIG. 6. Vortex links found in a three-dimensional slice of a 16^4 lattice universe, binned according to the extension of the cluster to which they belong (given in units of the maximal possible extension $\sqrt{3 \cdot 16^2}a/2$). Measurements were taken in the ensemble generated by the choice of coupling constants $\epsilon = 0.17, c = 0.4$ belonging to the non-confining regime, cf. Fig. 2. The distributions are normalized to unity, so that each bar represents the fraction of vortex links found in clusters of the corresponding extension.

VII. DISCUSSION

It is not surprising that the high temperature, deconfined phase of the vortex model is associated with a lack of vortex percolation in space slices of the universe. For any Polyakov loop correlator, one can choose a space slice containing both of the Polyakov loops involved as well as the minimal area spanned by them. Consider now the consequence of a lack of vortex percolation in this space slice in the following simple heuristic picture. Absence of percolation implies the existence of an upper bound d on the size of vortex clusters. Due to the closed nature of the vortex lines, this implies that, on the space-time plane containing the two Polyakov loops, any point at which a vortex pierces that plane comes paired with another such point at most a distance d away, cf. Fig. 7.

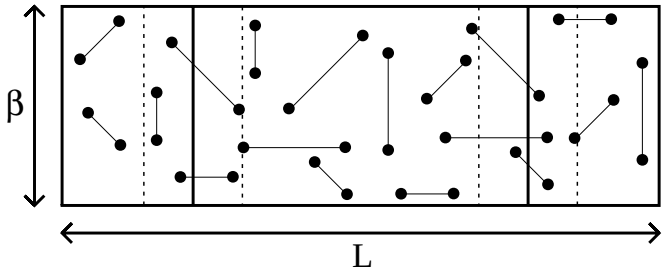

FIG. 7. Pairs of vortex intersection points of maximal separation d on a space-time plane. The thin lines connecting the points are merely to guide the eye in identifying the pairs. The existence of a maximal separation is a consequence of the vortices generating the intersection points being organized into clusters of maximal extension d in a higher dimension, i.e. these clusters do not percolate. Only pairs whose midpoints lie within the strips of width d (delineated by the interrupted lines) centered on the two Polyakov loops (solid lines) making up a Polyakov loop correlator have the possibility of contributing a factor (-1) to the latter.

Consider the idealized case of such pairs being randomly distributed on the space-time plane in question. Then one can evaluate the behavior of the Polyakov loop correlator at inverse temperature β on a universe of linear extension L as follows. Only pairs whose midpoints lie within the two strips of width d centered on the Polyakov loops can contribute a factor -1 to the Polyakov loop correlator. Denote by p the probability that such a pair actually does contribute a factor -1. This probability is an appropriate average over the distances of the midpoints of the pairs from the Polyakov loops, their angular orientations and the distribution of separations between the points making up the pairs. The probability p, however, does not depend on the macroscopic extension of the Polyakov loop correlator. Now, a pair which is placed at random on the space-time plane has probability $p \cdot A/\beta L$ of contributing a factor -1 to the Polyakov loop correlator, where $A = 2\beta d$ is the area of the two strips of width d centered on the Polyakov loops, and βL is the area of the entire plane. Placing N_{pair} pairs on the plane at random, the probability that n of them contribute a factor -1 to the Polyakov loop correlator is

$$P_{N_{pair}}(n) = \left(\begin{array}{c} N_{pair} \\ n \end{array} \right) \left(\frac{2pd}{L} \right)^n \left(1 - \frac{2pd}{L} \right)^{N_{pair}-n} \tag{8}$$

and, consequently, the expectation value of the correlator for large universes is

$$\langle W \rangle = \sum_{n=0}^{N_{pair}} (-1)^n P_{N_{pair}}(n) = \left(1 - \frac{4pd}{L} \right)^{N_{pair}} \stackrel{N_{pair}\to\infty}{\longrightarrow} e^{-2\beta p d \rho} \tag{9}$$

where the planar density of points $\rho = 2N_{pair}/\beta L$ is kept fixed as $N_{pair} \to \infty$. The Polyakov loop correlator is therefore independent of the separation between the Polyakov loops, negating confinement, if the extension of vortices or vortex networks in a space slice of the universe is bounded. Note that the persistence of percolation of the two-dimensional vortex surfaces as a whole in the deconfined phase does not influence this argument; what is important is the presence or absence of a pair correlation between vortex intersection points on the plane containing a Polyakov loop correlator.

Conversely, percolation of vortices is therefore a necessary condition for confinement. Only then is it possible for the points at which vortices pierce a given space-time plane to be sufficiently randomly distributed as to generate an area law for a Wilson loop or Polyakov loop correlator embedded in that plane; the pair correlation crucial in the model visualization presented above is no longer operative. Indeed, if one assumes these piercing points to be randomly distributed, one obtains by an argument analogous to the one above an area law with a string tension equal to twice the planar density of intersection points ρ, cf. [31]. More generally, if the points cannot be packed arbitrarily densely, but instead at most one per plaquette of a lattice (of spacing a) imposed on the plane can occur, the string tension obeys [18]

$$\sigma/\rho = -\frac{1}{\rho a^2} \ln(1 - 2\rho a^2) \tag{10}$$

which reduces to the value $\sigma/\rho = 2$ quoted above in the limit $a \to 0$.

The relation between the planar vortex density ρ and the string tension arising in the simple random picture (10) is obeyed to a good approximation by the values measured at zero temperature in the present vortex model (with $\epsilon = 0, c = 0.24$). At zero temperature, one has $\sigma a^2 = 0.755$ and $\rho a^2 = 0.27$, which fulfills (10) up to a 3% deviation; the measured quantities are thus consistent with a random distribution of vortex intersection points on any given space-time plane. The same behavior is found for the center projection vortices of Yang-Mills theory *after* subjecting them to a smoothing procedure [32]; the density of unsmoothed center projection vortices is significantly higher [24]. This is consistent with the physical interpretation discussed in section III. Quantitatively, the model vortex density quoted above differs from the center projection vortex density in SU(2) Yang-Mills theory [24] by a factor two.

The necessity of percolation for an area law behavior of the Wilson loop furthermore explains the persistence of percolation in time slices in the deconfined phase. Otherwise, spatial Wilson loops, which can be embedded in a time slice, could not continue to obey an area law above the deconfinement temperature. On the other hand, spatial Wilson loops can also be embedded in space slices, in which percolation ceases in the deconfined phase. The reason one can nevertheless still understand the spatial string tension in the space slice picture lies in the different topological setup: Vortices winding in the Euclidean time direction, which dominate the deconfined phase, pierce spatial Wilson loops at isolated points despite being of limited extension. The pair correlation between the piercing points which would preclude an area law does not arise due to the possibility of closing a short vortex line via the periodic boundary conditions.

To sum up, in the vortex picture there is a strong connection between confinement and the percolation properties of vortices. Percolation is a necessary condition for confinement; the deconfinement transition is induced by a percolation

transition to a phase which lacks percolating vortex clusters (when an appropriate slice of the configurations is considered). Also in this respect, the behavior of the vortex model presented here closely parallels the behavior found for the center projection vortices of Yang-Mills theory [25]. This connection between percolation and confinement moreover is one of the points at which the duality between the (magnetic) vortex picture and electric flux models becomes apparent. In electric flux models, the deconfinement transition also takes the guise of a percolation transition [39]; however, it is the *deconfined* phase in which electric flux percolates.

While this clarifies *how* vortex configurations generate the confined and deconfined phases, the simple structure of the vortex model investigated in this work also allows an intuitive understanding of the underlying dynamics, i.e. *why* the vortices behave as they do. Qualitatively, the parameters entering the vortex action have the following effects. The action per plaquette area ϵ (cf. eq. (4)) acts as a chemical potential for the mean density of vortices, whereas the curvature penalty c (cf. eq. (5)) imposes an ultraviolet cutoff on the space-time fluctuations of the vortex surfaces. To a certain extent, the two effects can be traded off with one another; striking evidence of this is provided by the approximately invariant physics found on the $T_c/\sqrt{\sigma_0} \approx 0.69$ trajectory depicted in Fig. 2. This can be understood as follows: If one generates two vortex configurations at random, then in all but exceptional cases, the configuration with the higher mean vortex density will also contain the higher amount of total curvature. Therefore, both coupling constants ϵ and c simultaneously curtail both the mean vortex density and the curvature. If one raises either ϵ or c, the mean density of vortices falls (and, along with it, the zero-temperature string tension). This gradual decrease of the string tension with the density does not persist indefinitely; instead, at some point, the vortex density becomes so low that the vortex structures lose their connectivity and form isolated clusters instead of percolating throughout space-time, cf. Fig. 6. This implies a pair correlation between vortex intersection points on a space-time plane which leads to an immediate loss of confinement, as already discussed further above. Therefore, despite there remaining a finite vortex density, the string tension vanishes; in this way, the confining and non-confining regions in Fig. 2 are generated.

Turning to the case of finite temperatures, the deconfining dynamics in the random vortex model can be understood in terms of an entropy competition. As one shortens the (lattice) universe in the Euclidean time direction, a new class of vortex clusters of small extension (viewed in a space slice) becomes available, namely the winding vortices which have been verified above to dominate the deconfined phase. Thus, the entropy balance between the class of percolating vortex configurations and the class of limited extension, non-percolating configurations shifts towards the latter. This interpretation of the deconfining dynamics is almost a tautology in view of the simple formal structure of the vortex model presented here. Evaluating the partition function (cf. eq. (1)) of the model by construction amounts precisely to enumerating all possible closed surface configurations, given a certain mean vortex density (enforced by the coupling constants ϵ and, indirectly, c) and an ultraviolet cutoff on the fluctuations of the vortex surfaces (embodied in the lattice spacing a and reinforced by the curvature penalty c). No other dynamical information enters the model, and therefore it can be nothing but the entropy associated with the different classes of random surfaces which determines which phase is realized.

VIII. OUTLOOK

In the previous sections, a model of infrared Yang-Mills dynamics was presented which allows an intuitive understanding of both the confinement phenomenon and the transition to a deconfined phase at finite temperatures. These properties are closely tied to the percolation characteristics of the vortex surfaces on which the model is based. The behavior of the random surface ensembles generating the two phases closely parallels the behavior found for center projection vortices in the Yang-Mills ensemble [25]. It is possible to choose the coupling constants of the vortex model such that long-range static quark potentials and spatial string tensions measured in Yang-Mills theory are quantitatively reproduced at all temperatures up to the cutoff of the model. The correct description of the spatial string tension in the deconfined phase should be noted in particular; this nontrivial feature at no point entered either the construction of the model or the choice of coupling constants.

The vortex model presented here was formulated to describe Yang-Mills theory with an SU(2) color group. The case of SU(3) color realized in nature will in some respects exhibit qualitatively different behavior; the center vortex model appropriate for this gauge group is currently under investigation. Since there are two nontrivial center elements in the SU(3) group, namely the phases $e^{\pm i2\pi/3}$ (multiplied by the 3×3 unit matrix), one must allow for two distinct vortex fluxes. The main qualitative difference in the topology of vortex configurations is the presence of vortex branchings; a vortex carrying one type of vortex flux can split into two vortices carrying the other type of vortex flux, as long as flux conservation is respected.

On the other hand, to provide a comprehensive picture of the infrared sector of QCD, the vortex model must also be investigated with a view to describing the topological susceptibility of the Yang-Mills ensemble and the spontaneous

breaking of chiral symmetry. The manner in which vortex configurations generate a nontrivial Pontryagin index was recently clarified in [22]; the relevant properties are encoded in the (oriented) self-intersection number of the vortex surfaces. In a companion paper [28], those results are implemented on a space-time lattice, allowing a measurement of the topological susceptibility. Also for this quantity, the vortex model generates a realistic value, compatible with lattice measurements in full SU(2) Yang-Mills theory. In the same vein, it is necessary to construct efficient ways to evaluate the spectrum of the Dirac operator in a vortex background. This will make it possible to calculate the associated chiral condensate [41], which represents an order parameter for the spontaneous breaking of chiral symmetry.

As a last remark, it is tempting to speculate that the phase diagram of electroweak theory [42] can similarly be understood in terms of the percolation characteristics of electroweak vortices [43], in particular as far as the confinement properties are concerned. In the Higgs phase, the coupling to the Higgs condensate may penalize the vortex density to such an extent that the theory enters the non-percolating, non-confining regime (the shaded region in Fig. 2), thus allowing electroweak gauge bosons to be seen as asymptotic states.

IX. ACKNOWLEDGEMENTS

M.E. thanks B.Petersson and G.Thorleifsson for an illuminating discussion on random surface models.

---

[1] H. J. Rothe, *Quantum Gauge Theories: An Introduction* (World Scientific, Singapore, 1997).
[2] G. 't Hooft, Nucl. Phys. **B190** (1981) 455.
[3] S. Mandelstam, Phys. Rep. **23C** (1976) 245;
A. Kronfeld, M. Laursen, G. Schierholz and U.-J. Wiese, Nucl. Phys. **B293** (1987) 461;
T. Suzuki and I. Yotsuyanagi, Phys. Rev. **D 42** (1990) 4257;
G. S. Bali, V. Bornyakov, M. Müller-Preussker and K. Schilling, Phys. Rev. **D 54** (1996) 2863.
[4] G. 't Hooft, Nucl. Phys. **B138** (1978) 1.
[5] Y. Aharonov, A. Casher and S. Yankielowicz, Nucl. Phys. **B146** (1978) 256.
[6] J. M. Cornwall, Nucl. Phys. **B157** (1979) 392.
[7] G. Mack and V. B. Petkova, Ann. Phys. (NY) **123** (1979) 442;
G. Mack, Phys. Rev. Lett. **45** (1980) 1378;
G. Mack and V. B. Petkova, Ann. Phys. (NY) **125** (1980) 117;
G. Mack, in: *Recent Developments in Gauge Theories*, eds. G. 't Hooft et al. (Plenum, New York, 1980);
G. Mack and E. Pietarinen, Nucl. Phys. **B205** [FS5] (1982) 141.
[8] H. B. Nielsen and P. Olesen, Nucl. Phys. **B160** (1979) 380;
J. Ambjørn and P. Olesen, Nucl. Phys. **B170** [FS1] (1980) 60;
J. Ambjørn and P. Olesen, Nucl. Phys. **B170** [FS1] (1980) 265.
P. Olesen, Nucl. Phys. **B200** [FS4] (1982) 381.
[9] H. G. Dosch, Phys. Lett. **B190** (1987) 177;
H. G. Dosch and Yu. A. Simonov, Phys. Lett. **B205** (1988) 339.
[10] S. L. Adler, Phys. Rev. **D 23** (1981) 2905.
[11] M. Baker, J. S. Ball and F. Zachariasen, Phys. Rev. **D 51** (1995) 1968.
[12] A. A. Belavin, A. M. Polyakov, A. Z. Schwartz and Yu. S. Tyupkin, Phys. Lett. **B59** (1975) 85;
C. Callan, R. Dashen and D. Gross, Phys. Rev. **D 17** (1978) 2717.
[13] N. Seiberg and E. Witten, Nucl. Phys. **B426** (1994) 19.
[14] E. T. Tomboulis, Phys. Rev. **D 23** (1981) 2371;
E. T. Tomboulis, Phys. Lett. **B303** (1993) 103.
[15] L. Del Debbio, M. Faber, J. Greensite and Š. Olejník, Nucl. Phys. Proc. Suppl. **53** (1997) 141.
[16] L. Del Debbio, M. Faber, J. Greensite and Š. Olejník, Phys. Rev. **D 55** (1997) 2298.
[17] L. Del Debbio, M. Faber, J. Greensite and Š. Olejník, in: *New Developments in Quantum Field Theory*, eds. P. H. Damgaard and J. Jurkiewicz (Plenum Press, New York – London, 1998); hep-lat/9708023.
[18] L. Del Debbio, M. Faber, J. Giedt, J. Greensite and Š. Olejník, Phys. Rev. **D 58** (1998) 094501.
[19] T. G. Kovács and E. T. Tomboulis, Phys. Lett. **B463** (1999) 104.
[20] C. Alexandrou, M. D'Elia and P. de Forcrand, talk presented at the 17th International Symposium on Lattice Field Theory (LATTICE 99), Pisa, Italy, 29 June - 3 July 1999, hep-lat/9907028.

[21] C. Alexandrou, P. de Forcrand and M. D'Elia, talk presented at the 15th International Conference on Particles and Nuclei (PANIC 99), Uppsala, Sweden, 10-16 June 1999, hep-lat/9909005.
[22] M. Engelhardt and H. Reinhardt, Nucl. Phys. **B567** (2000) 249.
[23] M. Faber, J. Greensite, Š. Olejník and D. Yamada, JHEP **9912** (1999) 012.
[24] K. Langfeld, O. Tennert, M. Engelhardt and H. Reinhardt, Phys. Lett. **B452** (1999) 301.
[25] M. Engelhardt, K. Langfeld, H. Reinhardt and O. Tennert, Phys. Rev. **D 61** (2000) 054504.
[26] P. de Forcrand and M. D'Elia, Phys. Rev. Lett. **82** (1999) 4582.
[27] J. M. Cornwall, Phys. Rev. **D 61** (2000) 085012.
[28] M. Engelhardt, hep-lat/0004013.
[29] M. Faber, J. Greensite and Š. Olejník, Phys. Rev. **D 57** (1998) 2603.
[30] M. Faber, J. Greensite and Š. Olejník, Acta Phys. Slov. **49** (1999) 177.
[31] M. Engelhardt, K. Langfeld, H. Reinhardt and O. Tennert, Phys. Lett. **B431** (1998) 141.
[32] R. Bertle, M. Faber, J. Greensite and Š. Olejník, JHEP **9903:019** (1999).
[33] K. Langfeld, H. Reinhardt and O. Tennert, Phys. Lett. **B419** (1998) 317.
[34] J. Ambjørn, G. Koutsoumbas and G. K. Savvidy, Europhys. Lett. **46** (1999) 319.
[35] S. Bilke, hep-lat/9902001.
[36] M. Teper, hep-th/9812187.
[37] O. Kaczmarek, F. Karsch, E. Laermann and M. Lutgemeier, hep-lat/9908010.
[38] G. S. Bali, J. Fingberg, U. M. Heller, F. Karsch and K. Schilling, Phys. Rev. Lett. **71** (1993) 3059.
[39] A. Patel, Nucl. Phys. **B243** (1984) 411;
A. Patel, Phys. Lett. **B139** (1984) 394.
[40] E. Witten, Nucl. Phys. **B156** (1979) 269;
G. Veneziano, Nucl. Phys. **B159** (1979) 213.
[41] T. Banks and A. Casher, Nucl. Phys. **B169** (1980) 103.
[42] O. Philipsen, M. Teper and H. Wittig, Nucl. Phys. **B528** (1998) 379;
M. N. Chernodub, F. V. Gubarev, E.-M. Ilgenfritz and A. Schiller, Phys. Lett. **B434** (1998) 83.
[43] M. N. Chernodub, F. V. Gubarev, E.-M. Ilgenfritz and A. Schiller, Phys. Lett. **B443** (1998) 244;
M. N. Chernodub, F. V. Gubarev, E.-M. Ilgenfritz and A. Schiller, Nucl. Phys. Proc. Suppl. **73** (1999) 671.